Thermal Analysis of SMC Motors Using a Hybrid Model with Distributed Heat Sources

YouGuang GUO, *Member, IEEE*, Jian Guo ZHU, *Senior Member, IEEE*, and Wei WU

***Abstract*--This paper presents a hybrid thermal model with distributed heat sources for thermal analysis of SMC motors. The model uses a combination of lumped and distributed thermal parameters, which can be obtained from motor dimensions and thermal constants, etc. A comprehensive method is used to calculate the core loss in each part, combined with three-dimensional magnetic field finite element analysis. The thermal model is applied to calculate the temperature distributions in a claw pole permanent magnet motor with SMC stator.**

***Index Terms*—Claw pole motor, core loss, hybrid thermal model, magnetic field analysis, soft magnetic composite.**

I. Introduction

ELECTRICAL machines with soft magnetic composite (SMC) core are attracting increasing attention due to the material's unique characteristics such as isotropic magnetic and thermal properties, low eddy current loss, and nearly net-shape fabrication process with minimal if any further machining [1]. In order to obtain an economic utilization of materials and safe operation of the motor, it is necessary to predict with reasonable accuracy the temperature rise of internal parts including copper, magnets and SMC core.

Studies on the thermal behavior of electrical machines started quite a long time back. Lumped parameter thermal model [2,3] and finite element methods [4] have been used in the past. By using a proper thermal network, the temperatures of different parts of a machine can be predicted with satisfactory accuracy. When the temperatures in many different points are required with a greater accuracy, however, numerical methods such as the finite element analysis (FEA) should be considered.

This paper presents a hybrid thermal model for an accurate estimation of temperature distributions in a claw pole permanent magnet SMC motor. The proposed model uses a combination of lumped and distributed thermal parameters, which can be derived from the motor geometry, thermal and physical properties of the materials and the heat transfer coefficients [5]. The model consists of nodes distributed along the thermal path of the motors where the neighboring nodes are connected by thermal resistances. Thermal sources such as core loss, copper loss and friction and windage loss are allocated to each node according to its location in the model. The core loss distribution is calculated by separating the hysteresis (alternating and rotational, both purely circular and elliptical), eddy current and anomalous losses in each element, when the rotor rotates [6,7]. A thermal capacitor is assigned to each node to consider the thermal storage, enabling transient analysis.

The whole motor is modeled into many small solid elements according to its structure and the materials. The heat is assumed to transfer by conduction within and between solid elements, and by convection and radiation between the surfaces of a solid element and the air. The thermal resistances are computed by using Fourier's law of heat conduction and equations for heat convection, with known dimensions of the motor, thermal conductivities of different materials, and convective heat transfer coefficients between air and solid materials (moving or standstill). The thermal calculation is conducted by a post-processing code implemented in the commercial software ANSYS, which firstly computes the magnetic field distribution, core loss and other parameters.

II. Thermal Model Formulation

The partial differential equation of the heat conduction is known as

$$K_x \frac{\partial^2 T}{\partial x^2} + K_y \frac{\partial^2 T}{\partial y^2} + K_z \frac{\partial^2 T}{\partial z^2} + q^* = \rho C_P \frac{\partial T}{\partial t} \tag{1}$$

where K_x, K_y and K_z [W/(m·K)] are the thermal conductivities along X, Y and Z directions, respectively, q^* [W/m^3] is the power loss density, C_P [J/(Kg·K)] the specific heat, ρ [Kg/m^3] the mass density, T [K] the temperature distribution, and t [s] the time.

To consider all the three components of the heat flow at one point, the element in which that point is located, with a block shape, can be modeled by 6 thermal resistances and 7 nodes. Fig.1 shows the three dimensional (3D) heat conduction model of a solid element, where q_a [W] is the heat generated in the solid element, C_a [J/K] is the thermal capacitance associated with node a and R_x, R_y and R_z are the equivalent heat transfer resistances along the X, Y and Z axes, respectively.

At the central node a, (1) can be expressed in terms of the

Y.G. Guo and J.G. Zhu are with the Faculty of Engineering, University of Technology, Sydney, NSW 2007, Australia (e-mail: youguang.guo-1@ uts.edu.au, jianguo.zhu@ uts.edu.au).

W. Wu is with CSIRO Telecommunications and Industrial Physics, NSW 2070, Australia (e-mail: wei.wu@csiro.au).

temperatures at its adjacent nodes *b*, *c*, *d*, *e*, *f* and *g*

$$\frac{T_b - T_a}{R_{ab}} + \frac{T_c - T_a}{R_{ac}} + \frac{T_d - T_a}{R_{ad}} + \frac{T_e - T_a}{R_{ae}} + \frac{T_f - T_a}{R_{af}} + \frac{T_g - T_a}{R_{ag}} + q_a = \frac{C_a}{\partial t}(T_a' - T_a) \tag{2}$$

where T_a and T_a' are the current and future temperatures at node *a*, R_{ab}, R_{ac}, R_{ad}, R_{ae}, R_{af} and R_{ag} are the thermal resistances between nodes *a* – *b*, *a* – *c*, *a* – *d*, *a* – *e*, *a* – *f* and *a* – *g*, respectively.

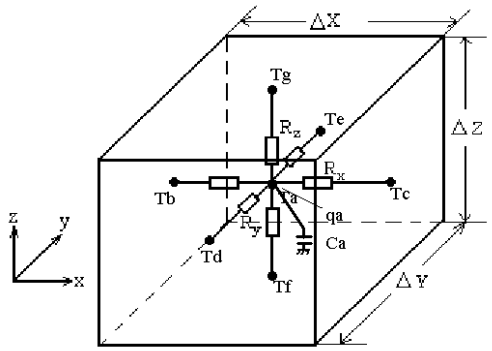

Fig. 1. Nodal network representation for three-dimensional heat flow

The thermal resistances can be calculated by

$$R_{ab} = R_{ac} = R_x = \frac{\Delta X}{2k_x \Delta Y \Delta Z} \tag{3a}$$

$$R_{ad} = R_{ae} = R_y = \frac{\Delta Y}{2k_y \Delta X \Delta Z} \tag{3b}$$

$$R_{af} = R_{ag} = R_z = \frac{\Delta Z}{2k_z \Delta X \Delta Y} \tag{3c}$$

The convection and radiation on a solid element surface can be evaluated by Newton's law of cooling, viz.

$$q = (h_c + h_r) A \Delta T \tag{4}$$

where q is the heat transferred, h_c and h_r are the coefficients of convection and radiation, respectively, A is the surface area, and ΔT the temperature difference between the surface and the surrounding air. The equivalent thermal resistance to the heat convection and radiation of the surface can be computed by

$$R_{cr} = \frac{1}{(h_c + h_r) A} \tag{5}$$

The whole motor can be modeled by a network of equivalent thermal resistances. The potential of a node is the temperature at that point, assuming the reference potential is the ambient temperature. The temperature rise of a node is defined as the difference between the node and the ambient temperatures.

III. Thermal Analysis in SMC Motors

A. The Claw Pole SMC Motor Prototype

To investigate the potential of SMC materials in manufacturing small motors of complex structures, a 3-phase PM claw pole motor with an SMC core has been designed and fabricated, as shown in Fig.2 [8]. The outer rotor comprises a tube of mild steel with an array of magnets for each phase mounted on the inner surface. Each stator phase has a single coil around an SMC core, which is molded in two claw pole discs. The major sizes include 94mm for the outside diameter, 93mm for the active axial length, 1.0mm for the main airgap, 40.5mm for the average diameter of the airgap, etc. The motor has been successfully operated at 2.65 Nm and 1800 rpm for a long time within the temperature limit, driven by a sensorless brushless DC controller.

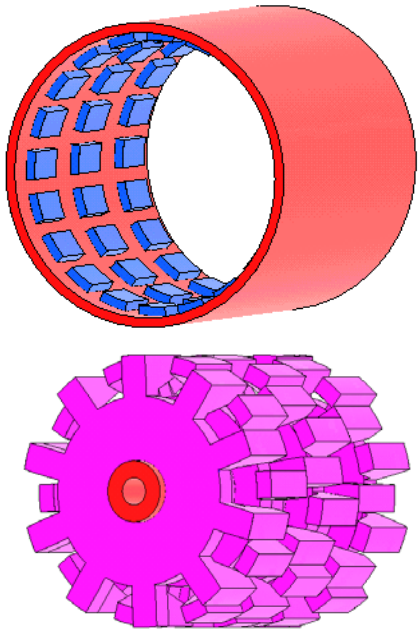

Fig. 2. Magnetically relevant parts of the claw pole motor

B. 3D Thermal Network

Because of the geometrical symmetry, only one pole pitch region of the motor needs to be considered in the thermal analysis, as shown in Fig.3 (the winding is not shown for clarity). Generally, a 3D equivalent heat transfer network is required. To simplify the calculation, the varnished copper winding can be considered as a homogeneous solid in the radial plane with an equivalent thermal conductivity and the heat conduction in the insulation layer between the stator core and the winding can be assumed one dimensional, that is, only the heat penetration in the direction of the thickness is considered.

A schematic diagram of thermal network is shown in Fig.4. To achieve a high accuracy, any part, e.g. the SMC stator claw pole, can be subdivided into as many segments as possible, as shown in Fig.5. Any irregular hexahedron, used for the solution region meshing, can be transformed to an equivalent block with six rectangular faces.

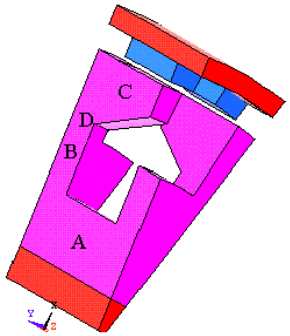

Fig.3 Region for thermal and magnetic field solutions

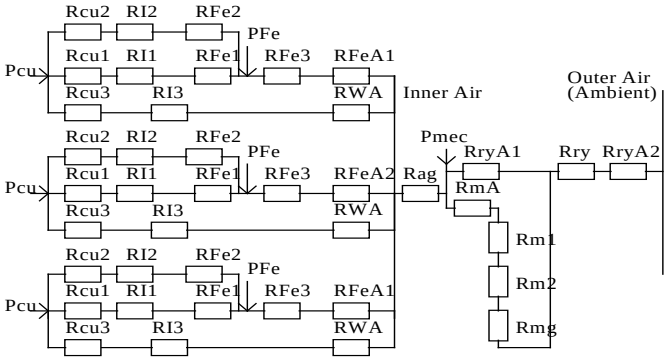

Fig.4 A schematic diagram of thermal network

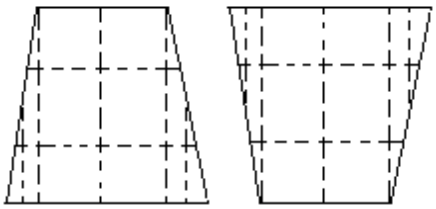

Fig.5 Claw-pole surface segments along both axial and circumferential directions

The conduction resistances in the following sections are calculated: rotor yoke (R_{ry}), magnets (R_m), air gap (R_{ag}), stator yoke (R_{Fe1}), stator claw pole discs (R_{Fe2}), stator claw poles (R_{Fe3}), varnished copper wire (R_{cu}) and insulations (R_{I1}, R_{I2}, R_{I3}) between the winding and the stator shaft, the stator claw pole disc and the air gap, respectively. In addition, the thermal resistances of the stator shaft (R_{ss}), the aluminum end plates (R_{al}) and the stationary air (R_{sa}) between the claw pole discs and the end plates are calculated separately.

The copper loss per phase (P_{cu}) can be evenly distributed to the winding region, the distribution of core loss per phase (P_{Fe}) is determined by the magnetic field analysis and the improved core loss model, and the mechanical loss (P_{mec}) is allotted to the air gap.

The soft magnetic composite material and the mild steel, used as the stator core and the rotor core, respectively, are thermally isotropic and hence $k_x=k_y=k_z$.

The thermal conductivities of different materials are chosen as: SMC=20, mild steel=50, air=0.027, aluminum=220, copper=380, magnet=9 and insulation=0.15. The diameter of the copper wire is 0.71 mm, which becomes 0.77 mm with varnish. The winding coil is considered as a homogeneous material in the plane perpendicular to the circumferential direction, with an equivalent thermal conductivity of 1.9 by

$$\frac{d_{cu,va}}{\lambda_{cu,va}}=\frac{d_{cu}}{\lambda_{cu}}+\frac{t_{va}}{\lambda_{va}} \tag{6}$$

where d_{cu} is the diameter of naked copper wire, t_{va} the thickness of varnish, $d_{cu,va}$ the diameter of the varnished copper wire and λ_{cu}, λ_{va} and $\lambda_{cu,va}$ are the thermal conductivities of the naked copper wire, varnish and varnished copper wire, respectively.

The equivalent thermal resistances to the heat convection (radiation in motor thermal analysis is usually ignored) of the following sections are calculated: between claw pole surface and inner air in the airgap (R_{FeA}), between winding and inner air (R_{WA}), between magnet and inner air (R_{mA}), between rotor yoke and inner air (R_{ryA1}), between rotor yoke and outer air (R_{ryA2}).

When the rotor is stationary, the natural convection between the rotor yoke surface and air is affected by the motion arising from differences in density between the heated air on the hot surface and the cooler and denser surrounding air. When the rotor rotates, the convection coefficient on the rotor outer surface is dependent on the velocity and is much higher than that in standstill. To determine the convection coefficient, the motor was operated with the rated load at the rated speed for 2 hours and the motor's surface temperature and input power were measured. The convection coefficient is calculated as the ratio of the input electrical power (the total power loss) and the product of the motor's surface area and temperature rise, namely 142 W/(m^{2}K) at 1800 rpm. The inner air is disturbed by the magnets and claw poles and the forced convection coefficient is calculated as 122 W/(m^{2}K) at 1800 rpm according to [9]

$$h=\frac{6.6}{10^5}\frac{v_r^{0.67}}{l_g^{0.33}}\quad \text{W/(cm}^2\cdot^o\text{C)} \tag{7}$$

where v_r [cm/s] is the velocity of the air and l_g [cm] the length of air gap. Note that this formula is used for the toothed structures based on the mean cylindrical area, and is valid only when the Reynolds number is larger than 200, which is calculated as 492 by $N_{re}=l_g v_r \rho/\mu$, where ρ is the mass density of air and μ the air dynamic viscosity. The Reynolds number of 492 indicates that the air in the air gap is turbulent and the thermal conductivity can be much larger than that of motionless air. The thermal resistance can be determined by

$$R_{ag}=\frac{l_g}{N_{nu}K_{air}A_{ag}} \tag{8}$$

where the Nusselt number $N_{nu}=0.155N_{re}^{0.7}$ [9], K_{air} is the

thermal conductivity of motionless air, and A_{ag} the average area of the air gap cylindrical surface.

C. Heat Sources

Because power losses are the inputs for temperature calculation, it is necessary to obtain reliable loss data and properly allot them to the corresponding nodes, in order to achieve good computation accuracy. The copper losses are computed from current and ohmic resistance, which is temperature dependent. The friction and windage loss is computed by empirical formula and validated by the "dummy stator test" of the prototype.

The iron losses are computed by a comprehensive method [6], which applies different formulations for iron loss prediction with purely alternating, purely circular rotating and elliptically rotating flux density vectors, respectively. A series of 3D finite element analyses is conducted to determine the flux density locus in each element in the claw pole SMC motor when the rotor rotates.

The magnetic circuits of three stacks (or phases) of the motor are basically independent. For each stack, because of the symmetrical structure, it is only required to analyze the magnetic field in one pole pitch, as shown in Fig.3 (the same as the region for thermal analysis).

At the two radial boundary planes of one pole pitch, the magnetic scalar potentials obey the so-called half-periodical boundary conditions:

$$\varphi_m\left(r,\Delta\theta/2,z\right)=-\varphi_m\left(r,-\Delta\theta/2,-z\right) \tag{9}$$

where $\Delta\theta = 18^o$ mechanical is the angle of one pole pitch. The original point of the cylindrical coordinate is located at the center of the stack.

As an example, Fig.6 plots the flux density locus in a typical element located in the middle of the claw pole and Fig.7 shows the time variations of three components of the flux density in the typical element. It can be seen that the magnetic field is really three-dimensional and the magnetic flux vector rotates in an elliptical pattern in a two-dimensional plane, which is not parallel to any coordinate axis.

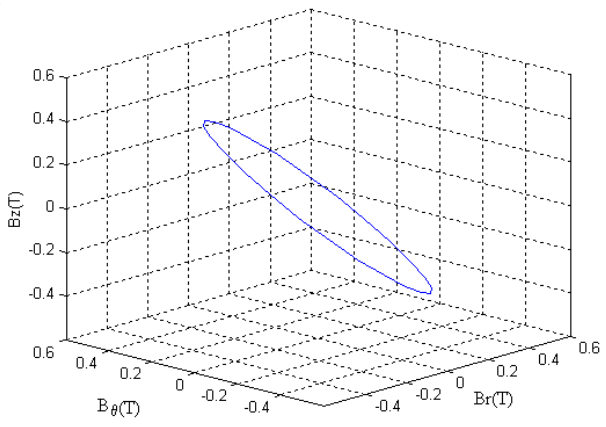

Fig.6 Flux density locus at Point C of Fig.3

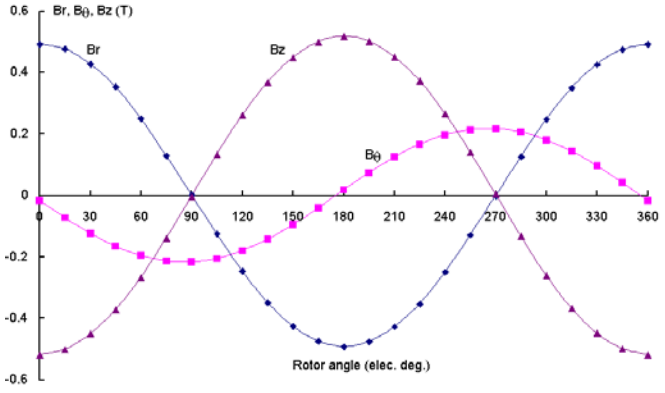

Fig.7 Time variation of flux density at Point C of Fig.3

Generally, the three components of flux density can be expressed as

$$B_r(\theta)=\sum_{k=0}^{\infty}\left(B_{rck}\cos\theta+B_{rsk}\sin\theta\right) \tag{10a}$$

$$B_\theta(\theta)=\sum_{k=0}^{\infty}\left(B_{\theta ck}\cos\theta+B_{\theta sk}\sin\theta\right) \tag{10b}$$

$$B_z(\theta)=\sum_{k=0}^{\infty}\left(B_{zck}\cos\theta+B_{zsk}\sin\theta\right) \tag{10c}$$

The magnitudes of the cosine and sine components of the k-th harmonic can be expressed, respectively, as

$$B_{ck}=\sqrt{B_{rck}{}^2+B_{\theta ck}{}^2+B_{zck}{}^2}\cos\theta \tag{11a}$$

$$B_{sk}=\sqrt{B_{rsk}{}^2+B_{\theta sk}{}^2+B_{zsk}{}^2}\sin\theta \tag{11b}$$

The locus of each harmonic flux density vector is an ellipse and the lengths of the major and minor axes, B_{kmaj} and B_{kmin}, correspond the magnitudes of the cosine and sine components of the harmonic, depending on which is larger.

In fact, the flux pattern in any element can be considered as elliptically rotating with harmonics (including purely circular and purely alternating). A series of finite element field analysis was conducted to find out B_{kmaj} and the axis ratio R_{BK} (=B_{kmin}/B_{kmaj}) in each element. The total core loss can then be calculated by

$$P_t=\sum_{e=1}^{Ne}\sum_{k=1}^{\infty}\left[P_{rk}R_{BK}+\left(1-R_{BK}\right)^2P_{ak}\right] \tag{12}$$

where N_e is the number of elements of the SMC stator, P_{ak} the alternating loss with flux density B_{kmaj}, determined by (13) and P_{rk} the purely rotational loss (R_{BK}=1), determined by (14-16).

$$P_{ak}=C_{ha}fB_{kmaj}{}^h+C_{ea}\left(fB_{kmaj}\right)^2+C_{aa}\left(fB_{kmaj}\right)^{1.5} \tag{13}$$

$$P_{ar}=P_{hr}+C_{er}\left(fB_{kmaj}\right)^2+C_{ar}\left(fB_{kmaj}\right)^{1.5} \tag{14}$$

$$\frac{P_{hr}}{f} = a_1\left[\frac{1/s}{(a_2+1/s)^2+a_3^2} - \frac{1/(2-s)}{[a_2+1/(2-s)]^2+a_3^2}\right] \quad (15)$$

$$s = 1 - \frac{B}{B_s}\sqrt{1-\frac{1}{a_2^2+a_3^2}} \quad (16)$$

where f is the frequency, C_{ha}, h, C_{ea} and C_{aa} are the coefficients for alternating hysteresis, eddy current and anomalous losses, respectively, P_{hr} is the rotational hysteresis loss, C_{er} and C_{ar} are the coefficients for the circularly rotational eddy current and anomalous losses, and a_1, a_2, a_3 and B_s are coefficients for the rotational hysteresis loss model. These coefficients can be determined by the curve fitting technique from the experimental data on SMC samples [6].

D. Thermal Calculation

After all the thermal resistances (or conductance) and capacitances are computed and the power losses are allotted to appropriate nodes, the node temperatures can be solved by

$$[G][T]+[P]=[C]\frac{d[T]}{dt} \quad (17)$$

where *[G]* is the inter-nodal conductance matrix, *[P]* is the power loss matrix, and *[C]* is a column matrix of thermal capacitance.

By using (17), the temperature distribution of the claw pole permanent magnet motor with SMC stator was calculated. The temperature rises at the middle points of several parts are listed in Table 1.

TABLE I
COMPARISON OF TEMPERATURE RISES BY HYBRID MODEL AND FEA

Temperatures rises (°C)	Hybrid model	FEA
Coil	74.3	72.2
Stator core	76.8	76.5
Airgap	55.2	53.5
Magnet	45.0	42.8
Rotor yoke outer surface	22.1	23.3

E. Thermal FEA

For comparison, the thermal FEA is also conducted by using the built-in program in ANSYS. The analysis region is taken as the same as that for magnetic field FEA, as shown in Fig.3. The core loss has been calculated based on elements, giving an accurate heat source distribution. The copper loss is uniformly allocated to the elements of coil, and the mechanical loss is evenly allocated to the airgap elements. Thermal parameters (material thermal conductivities and convection coefficients) and heat exchange conditions have been described in Section III(B). The calculation is conducted for the condition that the motor operates steadily with the rated torque and speed, and the calculated temperature rises are listed in Table 1.

The results obtained by the hybrid thermal model and by the thermal FEA are close. While the thermal FEA allows for easy modeling of complex shapes (e.g. take the same mesh as the magnetic field analysis) and is capable of producing accurate results, the proposed hybrid thermal model with distributed heat sources possesses the advantage of flexibility with acceptable accuracy and much reduced computational time. For example, for the steady analysis of this motor, it takes about 9 minute by FEA but only 17 seconds by the hybrid model. The time reduction is an important factor, especially when optimization is performed where a large number of iterations are required. The hybrid thermal model is easily implemented in the post-processor of ANSYS.

F. Temperature Measurement

When the prototype operated with the rated torque and speed at an ambient temperature of 20°C, the coil temperature was measured as 91°C by embedded thermocouples and the temperature on the rotor outer surface was measured as 43°C by an infrared temperature probe. The computed temperatures agree with the measurement.

IV. CONCLUSION

Thermal analysis, especially for non-conventional motors in which there is only limited knowledge about the temperature distribution, is a key issue in motor design. In this paper the thermal analysis has been conducted on a claw pole permanent magnet SMC motor by using a hybrid thermal model with lumped and distributed parameters. The core loss distribution is calculated by improved formulations combined with 3D magnetic field finite element analysis. The hybrid thermal model has the advantage of flexibility with reasonable accuracy, comparing with the finite element method and the conventional thermal network method.

REFERENCES

[1] A.G. Jack, "Experience with the use of soft magnetic composites in electrical machines," *Proc. Int. Conf. Electrical Machines*, Istanbul, Turkey, 1998, pp. 1441-1448.

[2] P.H. Mellor, D. Roberts, and D.R. Turner, "Lumped parameter thermal model for electrical machines of TEFC design," *Proc. Inst. Elect. Eng.*, pt. B, vol. 138, no. 5, pp. 205-218, Sept. 1991.

[3] N. Bianchi, S. Bolognani, and F. Tonel, "Thermal analysis of a run-capacitor single-phase induction motor," *IEEE Trans. Ind. Applicat.*, vol. 39, no. 2, pp. 457-465, Mar./Apr. 2003.

[4] G. Cannistrà, G. Cannistrà, and M. Silos Labini, "Thermal analysis in an induction machine using thermal network and finite element methods," in *Proc. IEE EMD Conf.*, 1991, pp. 300-304.

[5] S.C. Mukhopadhyay and S.K. Pal, "Temperature analysis of induction motors using a hybrid thermal model with distributed heat sources," *J. Appl. Phys*, vol. 83, no. 11, pp. 6369-6371, June 1998.

[6] Y.G. Guo, J.G. Zhu, J.J. Zhong, and W. Wu, "Core losses in claw pole permanent magnet machines with soft magnetic composite stators," *IEEE Trans. Magn.*, vol. 39, no. 5, pp. 3199-3201, Sept. 2003.

[7] J.G. Zhu and V.S. Ramsden, "Improved Formulations for Rotational Core Losses in Rotating Electrical Machines," *IEEE Trans. Magn.*, vol. 34, no. 4, pp. 2234-2242, July 1998.

[8] Y.G. Guo, J.G. Zhu, P.A. Watterson, W.M. Holliday, and W. Wu, "Improved design and performance analysis of a claw pole permanent magnet SMC motor with sensorless brushless DC drive," *IEEE Int. Conf. on Power Electronics and Drive Systems*, Singapore, Nov. 2003, pp. 704-709.

[9] D.B. Hoseason, "The cooling of electrical machines," *IEE Journal*, vol. 69, no. 409, Jan. 1931, pp. 121-128.